Bulletin of the Seismological Society of America, Vol. 100, No. 2, pp. 522–531, April 2010, doi: 10.1785/0120080369

Triggering Effect of M 4–5 Earthquakes on the Earthquake Cycle of Repeating Events at Parkfield, California

by Kate Huihsuan Chen, Roland Bürgmann, and Robert M. Nadeau

Abstract Stress perturbations influence earthquake recurrence and are of fundamental importance to understanding the earthquake cycle and determining earthquake hazard. The large population of repeating earthquakes on the San Andreas fault at Parkfield, California, provides a unique opportunity to examine the response of the repeating events to the occurrence of moderate earthquakes. Using 187 M −0.4 to ~1.7 repeating earthquake sequences from the High Resolution Seismic Network catalog, we find that the time to recurrence of repeating events subsequent to nearby M 4–5 earthquakes is shortened, suggesting triggering by major events. The triggering effect is found to be most evident within a distance of ~5 km, corresponding to static coseismic stress changes of $> 0.6 - 26.6$ kPa, and decays with distance. We also find coherently reduced recurrence intervals from 1993 to 1998. This enduring recurrence acceleration over several years reflects accelerated fault slip and thus loading rates during the early 1990s.

Online Material: Figures of event chronologies of RES, estimates of $dt+^*$, and coseismic static stress changes.

Introduction

Earthquake triggering is the process by which static and/or dynamic stress changes lead to other earthquakes at varying distance (Freed, 2005). Static stress changes induced by major events may explain the distribution of aftershocks, changes in seismicity rate, and the advance or delay of subsequent major events (e.g., Dieterich, 1994; King *et al.*, 1994; Harris, 1998; Stein, 1999; Hearn *et al.*, 2002; Freed and Lin, 2002). It has also been suggested that event triggering is due to dynamic stresses associated with seismic wave propagation (Rybicki *et al.*, 1985; Gomberg and Davis, 1996; Cotton and Coutant, 1997; Felzer and Brodsky, 2006). The importance of stress interaction for the distribution of recurrence intervals in a fault segment's earthquake cycle, however, is still unclear, due to the limited catalogs of recurring large earthquakes from historical or paleoseismic data (e.g., Console *et al.*, 2008). To better understand the degree to which stress interactions between earthquakes influence recurrence intervals, one needs statistically sufficient observations of repeating events in a natural fault system.

A characteristically repeating earthquake sequence (RES) is defined as a group of events with nearly identical waveforms, locations, and magnitudes and thus represents the recurring rupture of the same patch of fault. The recurrence intervals of repeating earthquake ruptures are sometimes found to be highly variable. The variation in recurrence times between events in a sequence can be represented by the coefficient of variation (COV, standard deviation of recurrence intervals divided by the mean). The COV can be higher than 0.30 due to a response to nearby earthquakes, a change in the strain rate, time-dependent or spatial variation in the frictional strength of the fault, variability in slip distributions of individual recurrences, or other effects, such as fluid pressure variations (e.g., Vidale *et al.*, 1994; Ellsworth, 1995; Marone *et al.*, 1995; Nadeau *et al.*, 1995; Schaff *et al.*, 1998; Peng *et al.*, 2005). Analysis of 17 M −0.7 to ~1.4 repeating earthquake sequences at Parkfield by Ellsworth *et al.* (1999) suggests a wide range of COV (0.11–0.87) with a median value of 0.33 (table 1 in Ellsworth *et al.*, 1999). Sykes and Menke (2006) studied the repeat times of global worldwide large earthquakes and found that the COV is smaller than 0.25 for the relatively simple plate boundaries, whereas the COV is larger than 0.5 for regions of multibranched faulting and overlapping slip near the ends of rupture zones.

The RESs at Parkfield, California, are believed to represent stick-slip asperities that are loaded and surrounded by the creeping San Andreas fault (e.g., Nadeau and Johnson, 1998). The questions of interest regarding the recurrence properties of natural earthquake sequences are: how do the characteristically repeating earthquakes respond to stress perturbations associated with larger earthquakes, and to what range (both in space and time) is triggering effective?

High Resolution Seismic Network (HRSN) Repeating Earthquake Sequences

The detailed record of microearthquake data from the borehole HRSN sites at Parkfield provides a unique opportunity to examine how larger events act on the observed occurrence of the repeating events. With the high level of detection of microearthquakes, the HRSN has revealed a large number of repeating earthquakes ranging in magnitude from −0.4 to +1.7 (e.g., Nadeau *et al.*, 1995). Locations of HRSN RES are shown in Figure 1. Recording of the HRSN deep borehole sensors began in early 1987, but the original data acquisition system failed in 1998. The HRSN network was upgraded with three new borehole stations installed in August 2001 (Nadeau *et al.*, 2004). Considering the two years of system shutdown, the study period is confined to 1987–1998. During the study period, we identified 187 RESs with a total event number of 1123.

During this observation period, five M 4.0–5.0 earthquakes ruptured along the Parkfield segment of the San Andreas fault: the 25 May 1989 (M 4.0), 20 October 1992 (M 4.6), 4 April 1993 (M 4.5), 14 November 1993 (M 5.0), and 20 December 1994 (M 5.0) events. The 187 RESs provide the opportunity to illustrate the triggering effect of these moderate earthquakes.

Hypocenters of the five M 4–5 earthquakes are shown in Figure 1. They are located close to the 1966 M 6 hypocenter except for the 1989 event. Fletcher and Spudich (1998) studied coseismic slip and rupture characteristics of the 20 October 1992, 14 November 1993, and 20 December 1994 earthquakes. The 14 November 1993 event, which occurred at the greatest depth, is characterized by the most active aftershock sequence and the simplest slip distribution with unclear directivity. The 1992 and 1994 events are characterized by fewer aftershocks and northward and slightly up-dip rupture propagation. Dashed red outlines in Figure 1 show the extent of the high-slip zones determined by Fletcher and Spudich (1998) for these three ruptures.

We consider the 187 HRSN RESs to address how the five M 4–5 earthquakes influence event timing. We evaluate changes in RES recurrence intervals associated with the times of the major events. This work relies on the correct identification of all repeating earthquake occurrences. Given that there is a possibility for missing repeating events, we emphasize the statistical pattern revealed from 187 RESs instead of that from any individual sequence.

Coherently Shortened Recurrence Intervals, 1993–1998

Figure 2a shows the RES event occurrences within 4 km of the 4 April 1993 M 4.5 earthquake hypocenter, which has the most RESs in its immediate vicinity. In Figures S1–S4 in Ⓔ the electronic edition of *BSSA*), we show time series of RESs near the other four M 4–5 events. Event chronologies of the RESs near the M 4.5 event shown in Figure 2a reveal coherently reduced recurrence times over several years (1993–1998, see also Fig. S5 in Ⓔ the electronic edition of *BSSA*). Within a distance of 10 km from the M 4.5 event, 85% of the RESs have shorter post-1993 recurrence intervals compared to the pre-1993 intervals. Figure 2b shows the ratios between the averaged recurrence intervals from

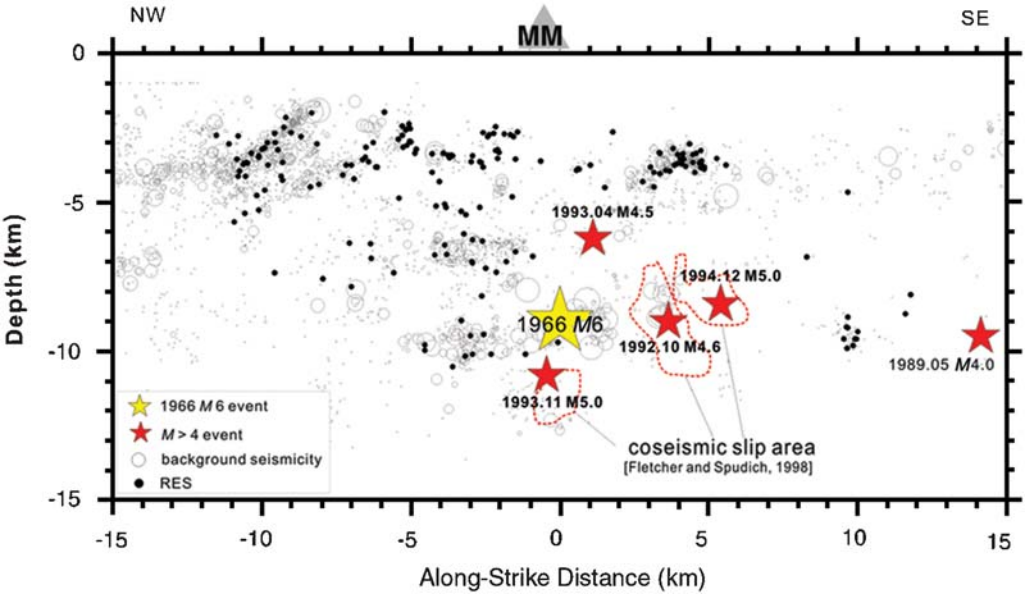

Figure 1. Along fault depth section, showing the distribution of 187 HRSN (1987–1998, black dots). Background seismicity (1987–1998, see Data and Resources section) is denoted by open circles. For reference, the 1966 M 6 hypocenter is indicated by a yellow star. M 4–5 earthquakes that occurred in the period of 1987–1998 are denoted by red stars. The size of a star refers to its magnitude. Slip models of the $M \geq 4.6$ events that occurred in October 1992, November 1993, and December 1994 by Fletcher and Spudich (1998) are outlined by red dashed lines.

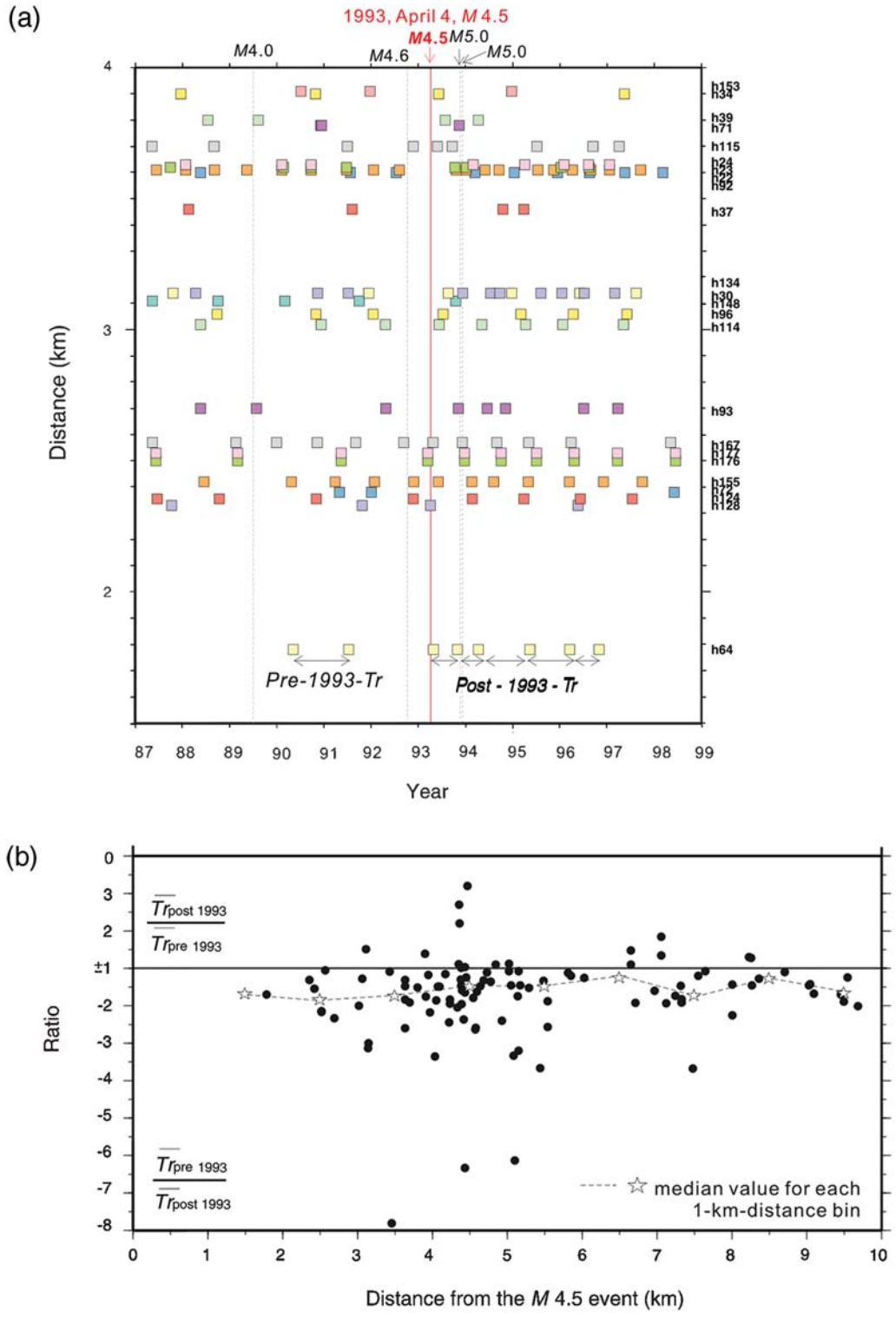

Figure 2. (a) Event chronologies of RESs as a function of distance from the 4 April 1993 M 4.5 hypocenter. Note that the distance is confined to be less than 4 km due to abundant RESs beyond 4 km. The vertical red line and arrow indicate the time of the 1993 M 4.5 event, whereas the other M 4–5 events in the study period are indicated by gray lines and arrows. (b) Ratio between mean post-1993 ($\bar{T}r_{\text{post1993}}$) and pre-1993 ($\bar{T}r_{\text{pre1993}}$) recurrence intervals as a function of distance from the 1993 M 4.5 event. The ratio is calculated as $\bar{T}r_{\text{post1993}}/\bar{T}r_{\text{pre1993}}$ for $\bar{T}r_{\text{post1993}} > \bar{T}r_{\text{pre1993}}$ and as $(-\bar{T}r_{\text{pre1993}}/\bar{T}r_{\text{post1993}})$ for $\bar{T}r_{\text{post1993}} < \bar{T}r_{\text{pre1993}}$, following Trotta and Tullis (2006), thus there are no values between -1 and 1. White stars represent the median of recurrence ratio for each 1-km-distance bin.

1993–1998 events and 1987–1993 events as a function of distance from the April 1993 M 4.5 hypocenter. Large negative values indicate a high degree of shortening of recurrence intervals in the post-1993 period. The difference between mean pre- and post-1993 recurrence intervals is largest for several sequences within shorter distances (< 5 km). The RES recurrence acceleration, however, is also evident at much larger distances. To further clarify to what degree the accelerated recurrences are a localized acceleration of creep due to the 1993 M 4.5 event, we calculate the median of the recurrence ratio for each 1-km-distance bin, as shown by white stars in Figure 2b. The median ratio shows a consistently negative ratio with distance, which implies a coherent acceleration. Also note that the median ratio does not systematically vary with distance, suggesting that the enduring acceleration of creep does not appear to be localized due to a close M 4–5 event, but is broadly distributed.

The distribution of recurrence intervals of the full RES data set also reveals a shortened recurrence interval in the post-1993 period. Figure 3 shows the distribution of recurrence intervals for 1987–1993 events, 1993–1998 events, and overall repeating events from 1987 to 1998. The post-1993 events tend to have shorter than two-year intervals with a mean value of 0.92 yr whereas the pre-1993 and full set of events have broad distributions of recurrence intervals in a range of 0.2 to 5 yrs and mean values of 1.8 yr, suggesting that the slip rate acceleration is by about a factor of 2. Both Figures 2 and 3 indicate an enduring recurrence acceleration since 1993, which encompasses much of the repeating events population we study. This is consistent with the view that there was a coherent slip transient along the Parkfield segment during this time period (e.g., Langbein *et al.*, 1999; Nadeau and McEvilly, 1999; Gao *et al.*, 2000; Murray and Segall, 2005).

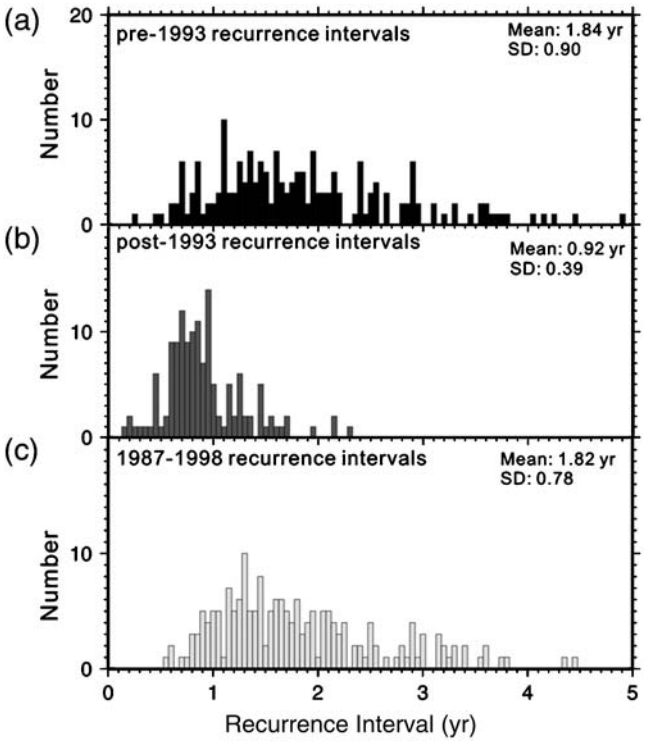

Figure 3. Histograms of recurrence intervals of the 187 Parkfield RESs determined from (a) pre-1993, (b) post-1993, and (c) full-period repeating events.

Recurrence Elements Associated with M 4–5 Events

To quantify the impact of M 4–5 events on an RES's timing, we consider five recurrence elements (Fig. 4) for the following analyses: (1) $dt+$, the time difference between a major earthquake and the first subsequent recurrence of a repeating event; (2) $dt-$, the time difference between a major earthquake and the most recent repeating event; (3) Tr_{cos}, the recurrence interval spanning the major event (i.e., the sum of $dt-$ and $dt+$); (4) Tr_{post}, the duration of the first full recurrence interval following the major event; and (5) Tr_{pre}, the last recurrence interval just preceding the potential trigger. These elements are divided by the average 1987–1998 recurrence interval of a given RES to obtain the normalized values of $dt+^*$, $dt-^*$, Tr^*_{cos}, Tr^*_{post}, and Tr^*_{pre}.

For each RES, the five recurrence elements associated with every M 4–5 event are calculated. In Figure 5a, the RES within 5 km distance from the major events tend to have a high fraction of short $dt+^*$. Figure 5a also shows the percentage of events within a given distance range that have a $dt+^*$ less than the threshold specified. For example, more than 30% of the nine events within 2 km distance have $dt+^* < 0.01$ (corresponding to $dt+$ of 0.36–1.46 days), whereas, within distances greater than 4 km, less than 10% of the 703 events exhibit such rapid recurrence. The percentage of short $dt+^*$ does not change for events within distances greater than 5 km. To confirm that the observed short $dt+$ population indicates the triggering effect of

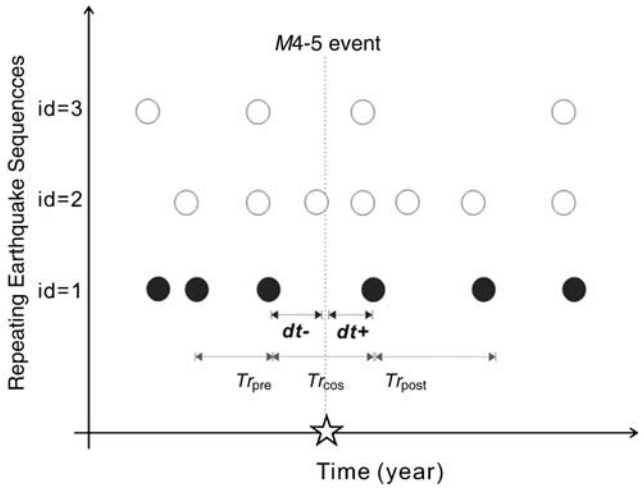

Figure 4. Schematic illustration of the five recurrence elements, $dt+$, $dt-$, Tr_{pre}, Tr_{cos}, and Tr_{post}.

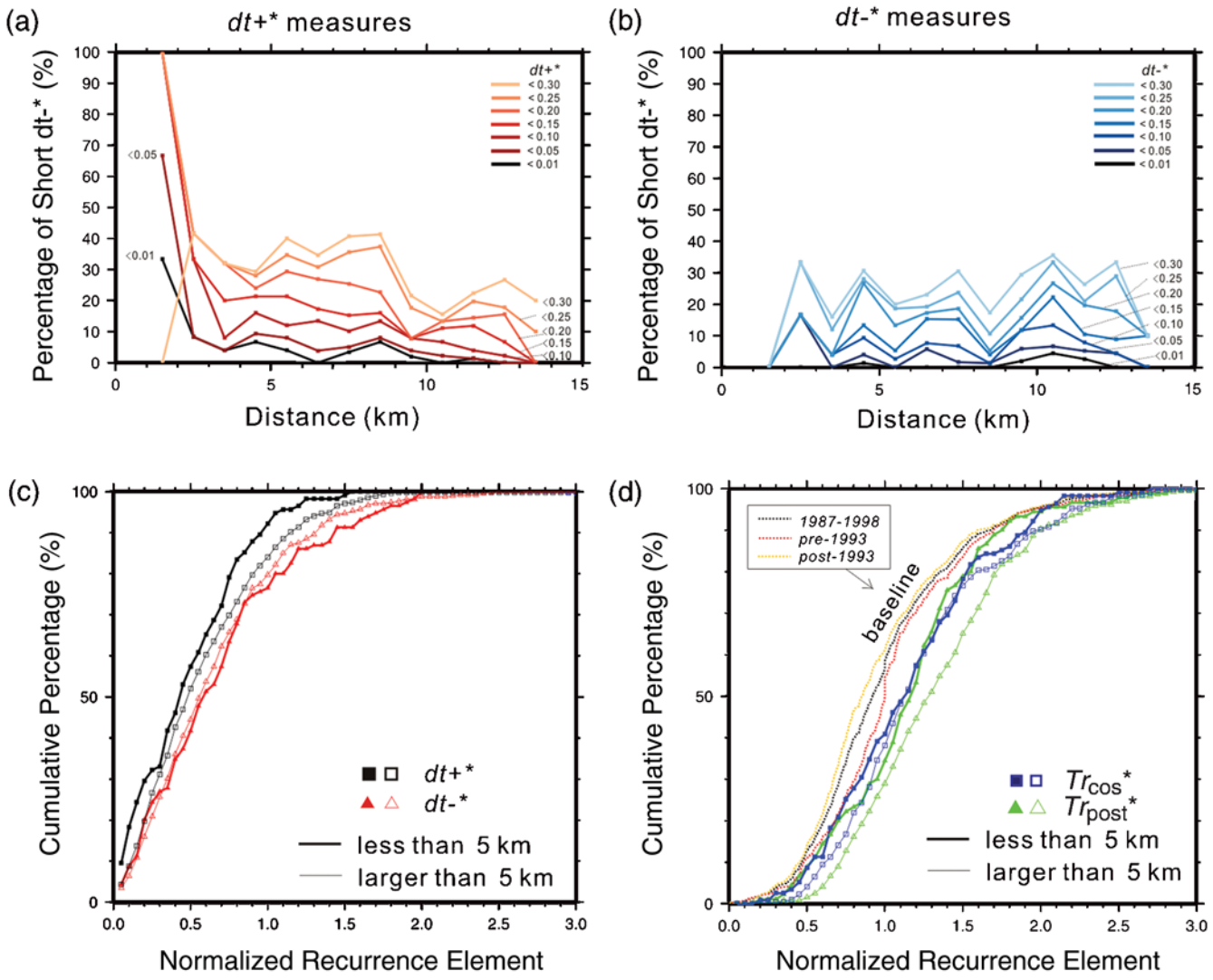

Figure 5. (a) Percentage of short $dt+^*$ as a function of distance from an M 4–5 event. Plotted values give percentages of events with $dt+^*$ that are shorter than the label on the color-coded lines. (b) Percentage of short $dt-^*$ as a function of interevent distance between the M 4–5 event and the RES. Lines are labeled with $dt-^*$ similar to those in (a). (c) Cumulative percentage of normalized recurrence element $dt+^*$ (black) and $dt-^*$ (red) at a distance of less (thick line) and greater (thin line) than 5 km. (d) Cumulative percentage of $Tr^*_{\cos}$ (blue) and Tr^*_{post} (green) at a distance of less (thick line) and greater (thin line) than 5 km. Black, orange, and yellow lines indicate background distribution (i.e., recurrence intervals without reference to the M 4–5 event locations and times) using the interval measurements during the whole (1987–1998), pre-1993 (1987–1993), and post-1993 (1993–1998) periods, respectively. Starred values of the elements indicate normalization by dividing these values with the mean recurrence interval of a given sequence.

M 4–5 events, we compare the observed distribution of $dt+^* < 0.1$, 0.1–0.2, and > 0.5 with $dt+^*$ values generated from randomly generated times of the five M 4–5 events. The 30 sets of five randomly generated M 4–5 times (150 runs in total) produce roughly equal percentages of $dt+^*$ at varying distance, as shown by blue lines in Figure 6. The random behavior of the small $dt+^*$ population ($dt^* < 0.1$) is strikingly different from the real population in the near field of the M 4–5 events (< 5 km). Beyond 5 km, however, the observed $dt+^* < 0.1$ distribution matches the synthetic $dt+^*$.

Compared to $dt+^*$ curves, Figure 5b shows the fraction of short $dt-^*$ measured over the same range of distances, which do not reveal systematic changes with distance. The percentages of the observed $dt-^*$ at all distances match the value of $dt-^*$, as one can expect from the random behavior. Figure 5c shows cumulative percentages of $dt+^*$ and $dt-^*$ at distances of less than and greater than 5 km from the M 4–5 hypocenters. As suggested by the analysis in Figure 5a, the distribution of $dt+^*$ is systematically shifted to smaller values at shorter distances from the source events. For example, 18.3% and 9.0% of $dt+^*$ have values of less than 0.1 within and outside of 5 km distance, respectively. The near-field $dt+^*$ curve in Figure 5c reveals a significant difference from the other three when the normalized recurrence element is smaller than 0.5. The short $dt+^*$ intervals subsequent to the M 4–5 events appear to be the result of

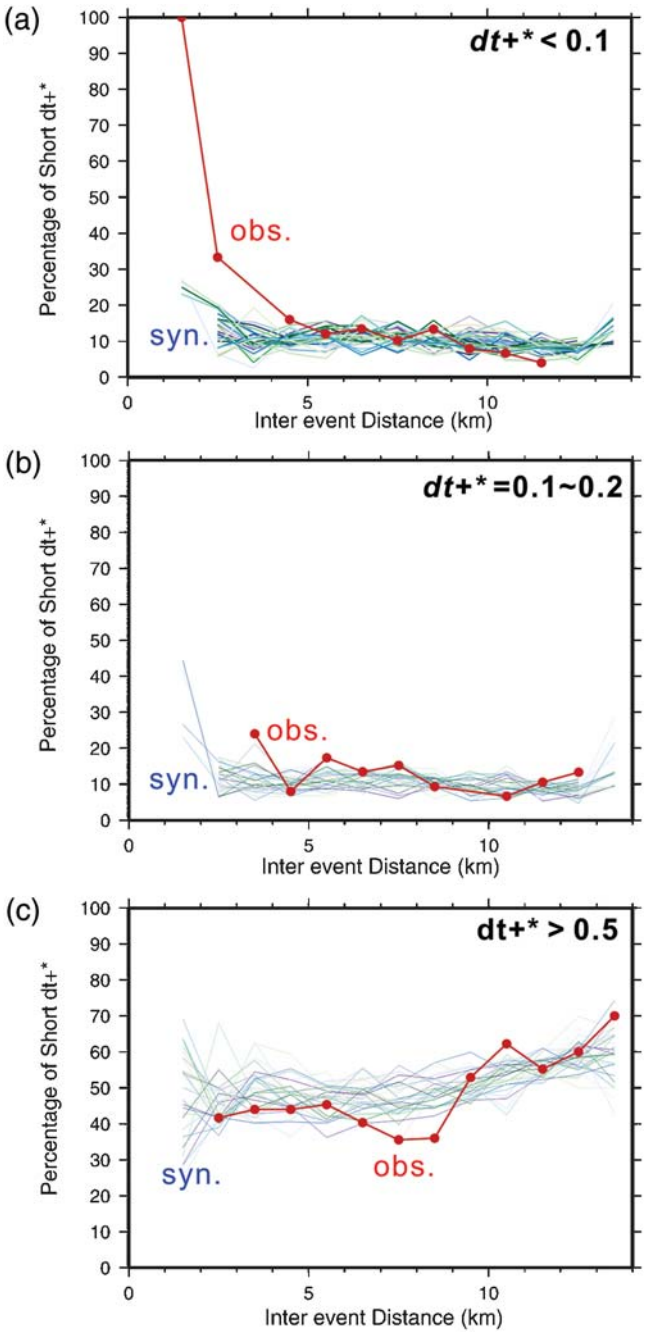

Figure 6. Percentage of (a) $dt{+}^* < 0.1$, (b) $0.1 \leq dt{+}^* < 0.2$, and (c) $dt{+}^* > 0.5$ as a function of distance from M 4–5 events for real data (red line) and synthetic data (blue lines generated by 30 sets of five randomly drawn M 4–5 event times). Note that the percentage in each distance bin (1 km) is calculated when the $dt{+}^*$ number greater than 3.

short distance triggering. The larger number of near-field $dt{-}^*$ is longer than 1.0, therefore the cumulative percentage for near-field $dt{-}^*$ appears to be the lowest in Figure 5c.

Fig 5d shows cumulative distributions of $Tr^*_{\cos}$ and Tr^*_{post} at distances of less than and greater than 5 km from the major events. The near-field RESs tend to have somewhat reduced $Tr^*_{\cos}$ and Tr^*_{post}; 8.5% of $Tr^*_{\cos}$ and 8.7% of Tr^*_{post} are shorter than 0.5 (i.e., recurrence within less than half of average interval), compared to 4.7% and 2.1% at >5 km distances. $Tr^*_{\cos}$ and Tr^*_{post} have mean values of 1.15 ± 0.49 (95% confidence interval) and 1.16 ± 0.48 for near-field events and 1.20 ± 0.53 and 1.18 ± 0.37 for events at distances greater than 5 km, respectively. These suggest that the reduction of the RES recurrence intervals spanning ($Tr^*_{\cos}$) and immediately following the M 4–5 events (Tr^*_{post}) is not statistically significant. When comparing the distribution of $Tr^*_{\cos}$ and Tr^*_{post} with that of all normalized recurrence intervals without reference to the M 4–5 event locations and times (shown with black dash-dotted line in Fig. 5d), we find that the normalized recurrence intervals spanning and immediately after the source events are actually larger than this baseline average. The longer $Tr^*_{\cos}$ and Tr^*_{post} can, in part, be a result of undetected repeating events, as discussed subsequently in the Undetected Repeating Events? section, and may also be the result of the coherently shortened recurrence intervals in 1993–1998.

Undetected Repeating Events?

As discussed in the previous section, the recurrence intervals of RESs spanning the M 4–5 events ($Tr^*_{\cos}$) are on average greater than the mean intervals and appear only modestly reduced at shorter distances (median value of 1.15 and 1.20 within and beyond 5 km distance, respectively). This may suggest the possibility that some triggered RES events occurred undetected immediately during the source earthquake. To understand whether the greater-than-1.0 $Tr^*_{\cos}$ indicates the effect of unrecognized repeating events, we examine the distribution of $Tr^*_{\cos}$ in comparison to Tr^*_{post} and Tr^*_{pre}.

In Figure 7, the histogram of Tr^*_{pre} reveals a somewhat broader distribution with a median value of 1.62. The median Tr^*_{pre} is about a half cycle longer than the median value of 1.14 and 1.29 for $Tr^*_{\cos}$ and Tr^*_{post}, respectively. This suggests a general pattern of shortened interval at and following the time of M 4–5 events. Note that the small secondary peak in Figure 7b is about twice the normalizing interval, indicating some missed recurrences that may have happened during the trigger event. The second peak at $Tr^*_{\cos} \sim 2$ is suggestive of a number of unrecognized repeating events. Because the secondary peak near 2 is minor, the undetected repeating events are unlikely to have significant influence on the M 4–5 triggering effect. Missing repeats in the Tr^*_{pre} and Tr^*_{post} distributions are also possible, as revealed by the subtle secondary peaks close to 1.9 in Figure 7a,c. Given that the secondary peaks are not as obvious as the $Tr^*_{\cos}$, we infer that the chance of undetected repeating events is more difficult to establish for pre- and postshock periods. We note that Tr^*_{post} is also somewhat reduced compared to pre-event recurrences, indicating the possible role of afterslip or general acceleration of slip in the early 1990s.

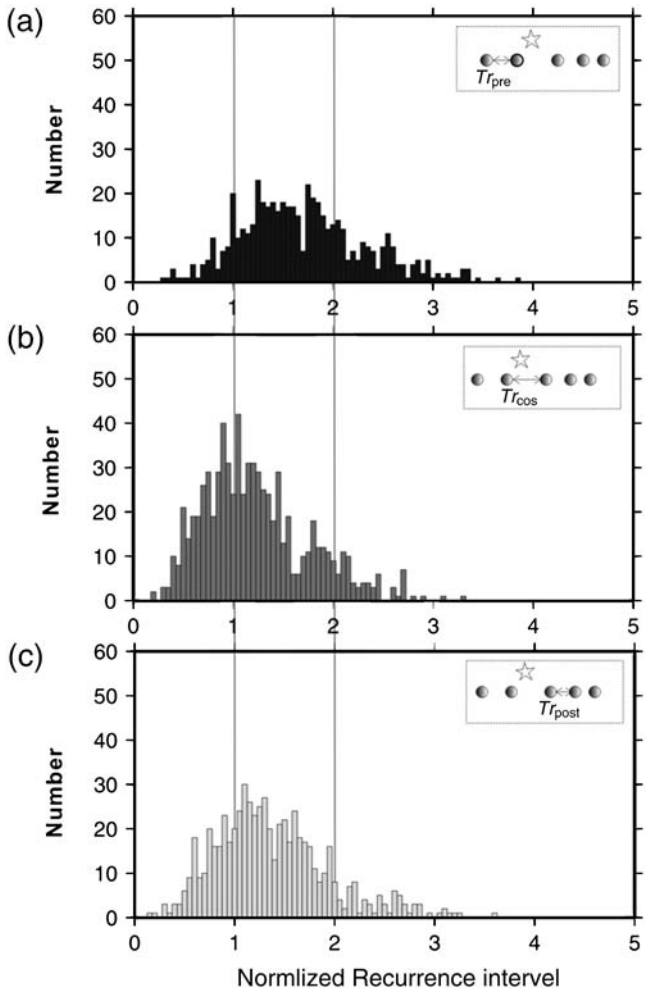

Figure 7. Histograms of Tr^*_{pre}, Tr^*_{cos}, and Tr^*_{post}, determined by the average recurrence intervals of full-period (Tr_{all}). Gray lines, normalized recurrence intervals of 1 and 2.

Are Triggered RESs Late in Their Earthquake Cycle?

To better understand the triggering effect on the recurrence intervals that span the time of the source event, we evaluate whether potentially triggered events (short $dt+^*$) tend to be late in their repeating earthquake cycle. To do this, we compare $dt+^*$ with the associated $dt-^*$ ($dt-^*$ from the same repeating sequence). A short $dt+^*$ along with high $dt-^*$ indicates that an event occurred in a late stage of the seismic cycle ($dt-^* \sim 1$). The distribution of $dt+^*$ and $dt-^*$ of RESs in three distance ranges from the M 4–5 events is shown in Figure 8. We divide the data space into four quadrants separated by lines $dt+^* + dt-^* = 1$ (i.e., Tr_{cos} is equal to the average recurrence time) and $dt+^* = dt-^*$ (i.e., the amount of time before the triggering event is equal to the amount of time after it). As listed in Table 1, events in quadrants A and D indicate the repeating events occurred early in the seismic cycle ($dt+^* > dt-^*$), whereas B and C indicate the events occurred late in the cycle ($dt+^* < dt-^*$). When the summation of $dt+^*$ and $dt-^*$ is shorter than the average recurrence interval, the data would fall in quadrants C and D. On the contrary, the data fall in quadrants A and B when the summation of $dt+^*$ and $dt-^*$ is longer than the typical cycle. Quadrants B and C indicate the events occurred in the later half of the cycle. To see the short $dt+^*$ late in its earthquake cycle, we expect the data to fall in quadrants B and C.

The percentage of data values in each quadrant is indicated by the numbers in boxes in Figure 8. The proportion of $dt+^* < dt-^*$ data is revealed by the sum in quadrants B and C, which increases from 46% to 59% and 61% when the distance decreases from >10 km, 5–10 km, to <5 km. The percentage of data points in quadrants C and D increases from 36% to 39% and 41% with decreasing distance from >10 km, 5–10 km, to <5 km. The five RESs that are located at distance <2.35 km are shown as filled stars in Figure 8b. All of these very-near-field events have $dt+^* < 0.1$. For distances longer than 2.35 km, some larger $dt+^*$ (> 0.5) start to occur, as shown in Figure 8b by the open stars in quadrants A and D for distances of 2.35–3.00 km. While the distribution of normalized recurrence intervals is very broad for all distance ranges, we find that the time to recurrence of the RES is decreased in closer vicinity to the M 4–5 earthquakes, especially for events further along in their earthquake cycle.

We also examine the $dt+^*$ versus $dt-^*$ relation using different choices of the average recurrence interval: pre-1993, post-1993, and full-period recurrence intervals. The result summarized in Table 1 reveals high variability in data percentage for the four quadrants A to D. The $dt+^*$ and $dt-^*$ determined by the post-1993 and full-period recurrence intervals have the greatest percentage of events in quadrant B for the <5 km and 5–10 km zones, indicating that the events within a distance of 10 km tend to be later and longer than their typical cycle. The $dt+^*$ and $dt-^*$ determined by the pre-1993 recurrence interval are dominant in quadrant C, indicating the events tend to be late and short relative to their own cycle. All three choices of average recurrence interval for the normalization have the largest percentage of data in either quadrants B or C, for the distance less than 10 km. This suggests that M 4–5 event triggering is more evident in the near field, and the triggering happened when the events were already late in their typical cycle. Beyond 10 km, there is likely no triggering because the dominant group is the early and long (or short) quadrant.

Static Triggering, Dynamic Triggering, or Change in Local Creep Rate?

Most likely, dynamic triggering, static triggering, or a transient increase of the creep rate play a role in RES recurrences. Differentiating one from another requires more detailed model investigations in the future. The recurrence elements analysis shown in this study, however, can provide useful information in this regard.

As illustrated in Figures 5a and 6a, the observed triggering effect is likely a function of interevent distance, where an accelerated occurrence of events is evident up to about 5 km

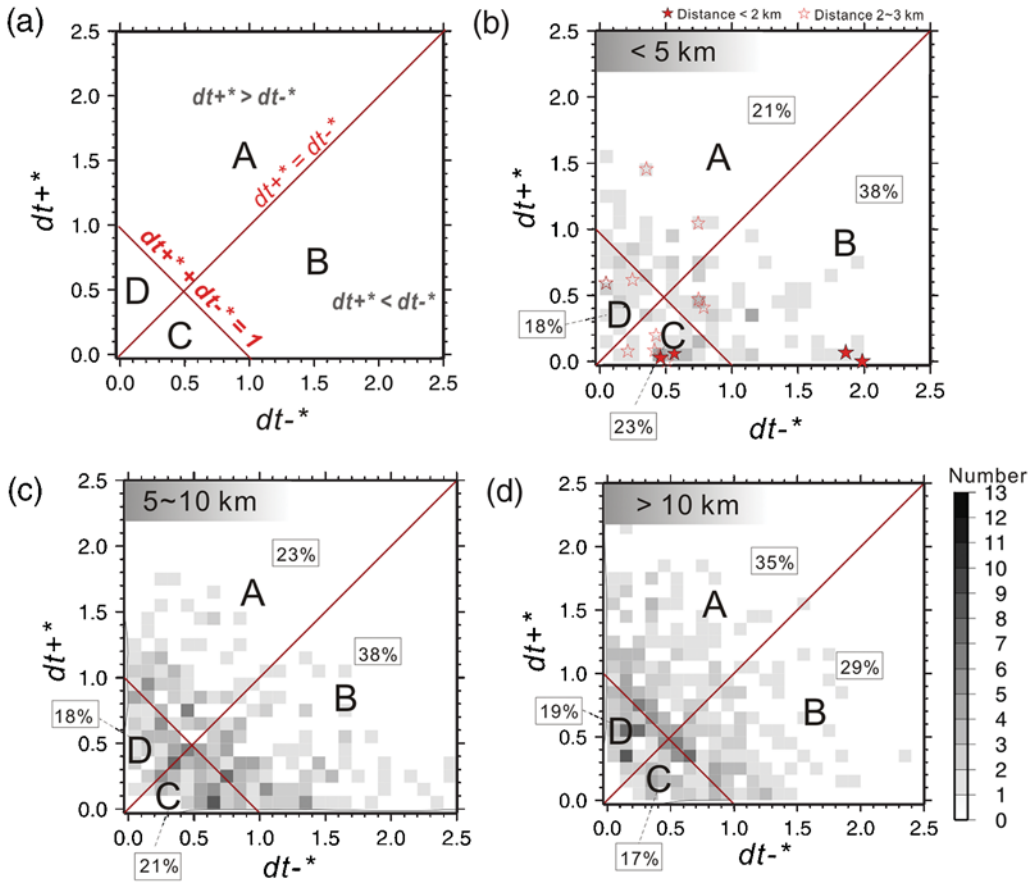

Figure 8. (a) Plot of $dt+^*$ versus $dt-^*$ for the RESs in distance range of (b) <5 km, (c) 5–10 km, and (d) >10 km from the M 4–5 events. Number of measures of ($dt+^*$, $dt-^*$) in each 0.1 × 0.1 cell are indicated by gray shaded squares and contour. Red straight lines represent $dt+^* + dt-^* = 1$ and $dt+^* = dt-^*$, respectively, which divide the space into A–D quadrants. Percentage of RES values in each quadrant is shown in the small boxes. Red filled and open stars in (b) represent the ($dt+^*$, $dt-^*$) measures for the distance range of <2.35 km and 2.35–3.00 km.

from the M 4–5 events. All events within 2.35 km occur within $dt+^* < 0.1$. For an M 5 event, static stress change from coseismic slip at 5 km distance is about 26.6 kPa (Fig. S6 in Ⓔ the electronic edition of *BSSA*), calculated using $\Delta\sigma = 1/6\pi Mo/r^3$, where r is the distance from the hypocenter (Aki and Richards, 1980) and Mo is seismic moment. More than 80% of very short $dt+^*$ measures (<0.1) experienced static stress change of >0.3 kPa, though some are associated with far-distance M 4–5 events, corresponding to static stress changes of <0.07 kPa. The limited influence zone (i.e., 3–5 times the rupture dimension of a moderate event) may imply that static stress increases from coseismic rupture and afterslip are likely to contribute to the observed acceleration of recurrence.

The possible role of dynamic triggering can be further illustrated by a significantly enhanced number of very short

Table 1

Percentage of Data Values in Four Quadrants of $dt+^*$ vs. $dt-^*$ Data Space

Choice of Average Recurrence Interval for Normalization	Distance to the M 4–5 Events	A Early & Long (%)	B Late & Long (%)	C Late & Short (%)	D Early & Short (%)
Recurrence intervals from 1987–1998 events ($\bar{T}r_{\text{all}}$)	<5 km	21.05	37.72	22.81	18.42
	5–10 km	22.88	38.23	21.24	17.65
	>10 km	34.82	28.57	17.56	19.05
Recurrence intervals from pre-1993 events ($\bar{T}r_{\text{pre1993}}$)	<5 km	0.88	0.88	59.65	38.60
	5–10 km	1.94	0.65	58.58	38.83
	>10 km	4.15	1.04	47.15	47.67
Recurrence intervals from post-1993 events ($\bar{T}r_{\text{post1993}}$)	<5 km	34.02	50.52	10.31	5.15
	5–10 km	33.96	55.04	5.78	5.22
	>10 km	40.41	37.82	17.62	4.15

$dt+^*$ out to larger distance. As shown in Figure 6a, the small $dt+^*$ population does not show strong favor for triggering at shorter distances. Comparing to the $dt+^*$ distribution by randomly chosen source times in Figure 6b, the distinction between the observed and synthetic curves disappears beyond 5 km, to match the percentage of 10%. The observed $>10\%$ small $dt+^*$ in the near field is likely to indicate the triggering effect of M 4–5 events because the triggering cannot be clearly seen out to great distance, which may indicate that dynamic triggering plays an insignificant role.

The role of creep rate changes can be indicated by the temporal variation of recurrence interval. Normalized recurrence interval versus time plot (Fig. 9) confirms a general pattern of lower creep rate in the pre-1993 period. However, normalized recurrence intervals tend to be shorter than 0.5 near 1990.5 and 1993.5–1994.5, which does not directly correspond with the timing of the M 4–5 events. Given the assumption that the average recurrence interval is inversely proportional to the average fault loading rate (Scholz, 1990; Nadeau and Johnson, 1998; Schaff *et al.*, 1998; Beeler *et al.*, 2001), the shortened normalized recurrence interval pattern in Figure 9 suggests that the increase in creep rate is not necessary to correlate with individual M 4–5 events. The large distance and long duration over which recurrence intervals are reduced suggests that this is unlikely to be the result of simple event triggering by stress increases from coseismic slip or afterslip. A transient increase in geodetically derived fault slip rate, seismicity rate, and RES recurrence–derived deep slip rate was observed during the same period of time (e.g., Langbein *et al.*, 1999; Nadeau and McEvilly, 1999; Gao *et al.*, 2000; Murray and Segall, 2005). Thus, the enduring recurrence acceleration over several years was part of a more broadly distributed increase in creep rates along this fault segment. It is possible that the M 4–5 events during this time were triggered by and further enhanced this transient slip event.

Summary

We illustrated the effect of moderate events on earthquake cycles of nearby characteristically repeating microearthquakes and determined the distance over which triggering can be documented. We found evidence that the five M 4–5 events that occurred at Parkfield from 1993 to 1998 triggered small, nearby repeating earthquakes. A high percentage of repeating events that occurred subsequent to the M 4–5 events within a distance of 5 km happened within a small fraction of their own average recurrence interval. The M 4–5 events also shortened the RES earthquake cycles spanning or immediately following their occurrence. In addition, we found that only events that are relatively late in their respective earthquake cycle get triggered. That is, the M 4–5 events trigger small repeating events that are approaching critical conditions for rupture. In future work, we will consider whether interaction with nearby $M<4$ events plays an additional important role in RES recurrence patterns. We will also explore in detail the response of the RESs to the M 6 2004 Parkfield earthquake.

Data and Resources

Repeating earthquake data used in this article came from published sources listed in the references. Plots were made using the Generic Mapping Tools version 4.2.1

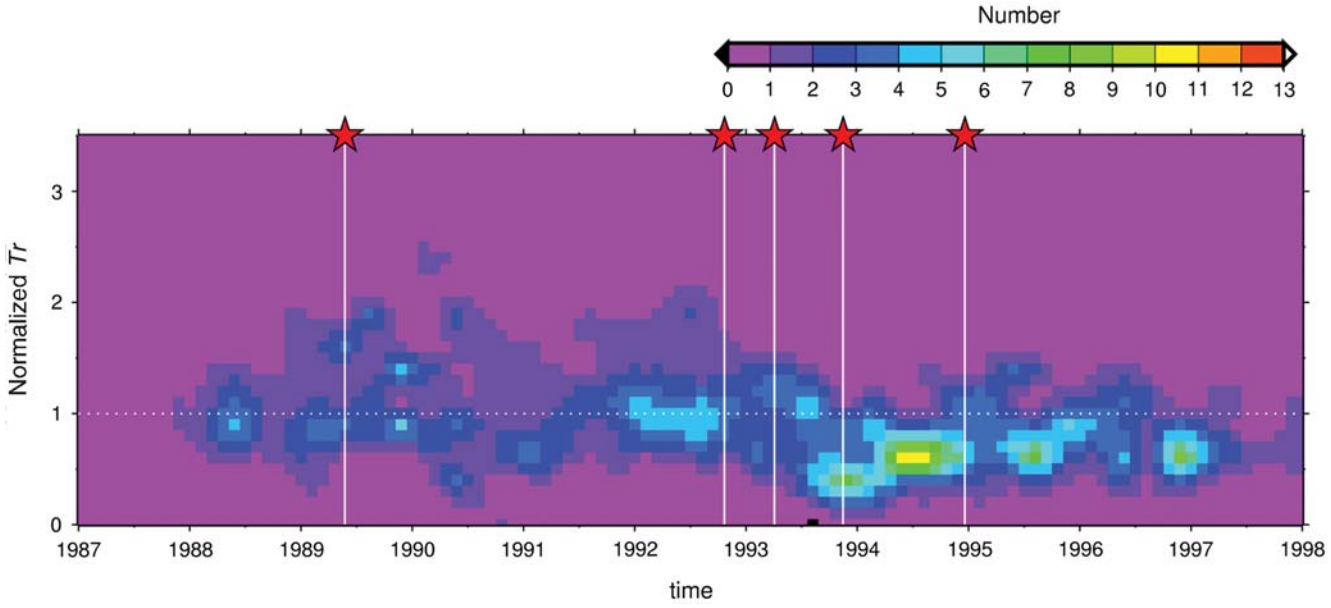

Figure 9. Density plot of normalized recurrence interval as a function of time. Horizontal dashed line, average recurrence interval; vertical solid line, timing of M 4–5 events. Recurrence intervals between events are normalized by the average recurrence interval from the 1987–1998 events.

(www.soest.hawaii.edu/gmt; Wessel and Smith, 1998). Catalog data for the background seismicities used in Figure 1 (1987–1998) are available at http://www.ncedc.org/hrsn/hrsn.archive.html.)

Acknowledgments

We are grateful to Bruce Shaw, Terry Tullis, and Justin Rubinstein for helpful discussions. We also thank Grant Dexter for English corrections. Terry Tullis and an anonymous reviewer provided thorough and helpful reviews. This work was funded by a Southern California Earthquake Center grant, contribution number 1338. The High Resolution Seismic Network (HRSN) is operated by the Berkeley Seismological Laboratory with support from Advanced National Seismic System grants 07HQAG0014 and National Science Foundation grants EAR-0537641, EAR-0544730, and EAR-0738342. Berkeley Seismological Laboratory contribution number is 09-13.

References

Aki, K., and P. G. Richards (1980). *Quantitative Seismology: Theory and Methods*, W. H. Freeman and Co., New York, 932 pp.

Beeler, N. M., D. L. Lockner, and S. H. Hickman (2001). A simple stick-slip model for repeating earthquakes and its implication for microearthquakes at Parkfield, *Bull. Seismol. Soc. Am.* **91,** 1797–1804.

Console, R., M. Murru, G. Falcone, and F. Catalli (2008). Stress interaction effect on the occurrence probability of characteristic earthquakes in Central Apennines, *J. Geophys. Res.* **113,** no. B08313, 1–18, doi 10.1029/2007JB005418.

Cotton, F., and O. Coutant (1997). Dynamic stress variations due to shear faults in a plane-layered medium, *Geophys. J. Int.* **128,** 676–688.

Dieterich, J. H. (1994). A constitutive law for rate of earthquake production and its application to earthquake clustering, *J. Geophys. Res.* **99,** 2601–2618.

Ellsworth, W. L. (1995). Characteristic earthquakes and long-term earthquake forecasts, implications of central California seismicity, in *Urban Disaster Mitigation:The Role of Science and Technology*, F. Y. Cheng and M. S. Sheu (Editors), Elsevier Science Ltd., Amsterdam, 1–14.

Ellsworth, W. L., M. V. Matthews, R. M. Nadeau, S. P. Nishenko, P. A. Reasenberg, and R. W. Simpson (1999). A physically based earthquake recurrence model for estimation of long-term earthquake probabilities, *U.S. Geol. Surv. Open-File Rept. 99–522*, 22 pp.

Felzer, K. P., and E. E. Brodsky (2006). Decay of aftershock density with distance indicates triggering by dynamic stress, *Nature* **441,** 735–738.

Fletcher, J. B., and P. Spudich (1998). Rupture characteristics of the three *M* 4.7 (1992–1994) Parkfield earthquakes, *J. Geophys. Res.* **103,** 835–854.

Freed, A. M. (2005). Earthquake triggering by static, dynamic, and postseismic stress transfer, *Ann. Rev. Earth Planet. Sci.* **33,** 335–367.

Freed, A. M., and J. Lin (2002). Accelerated stress buildup on the Southern San Andreas Fault and surrounding regions caused by Mojave Desert earthquakes, *Geolog* **30,** 571–574.

Gao, S., P. G. Silver, and A. T. Linde (2000). Analysis of deformation data at Parkfield, California: Detection of a long-term strain transient, *J. Geophys. Res.* **105,** no. B2, 2955–2967.

Gomberg, J., and S. Davis (1996). Stress/strain changes and triggered seismicity at The Geysers, California, *J. Geophys. Res.* **101,** 733–749.

Harris, R. A. (1998). Introduction to special section: Stress triggers, stress shadows, and implications for seismic hazard, *J. Geophys. Res.* **103,** 24,347–24,358.

Hearn, E. H., R. Bürgmann, and R. E. Reilinger (2002). Dynamics of Ízmit earthquake postseismic deformation and loading of the Düzce earthquake hypocenter, *Bull. Seismol. Soc. Am.* **92,** 172–193, doi 10.1785/0120000832.

King, G. C. P., R. S. Stein, and J. Lin (1994). Static stress changes and the triggering of earthquakes, *Bull. Seismol. Soc. Am.* **84,** 935–953.

Langbein, J., R. Gwyther, R. Hart, and M. Gladwin (1999). Slip rate increase at Parkfield in 1993 detected by high-precision EDM and borehole tensor strain meters, *Seismol. Res. Lett.* **26,** 2529–2532.

Marone, C., J. E. Vidale, and W. Ellsworth (1995). Fault healing inferred from time dependent variations in source properties of repeating earthquake, *Geophys. Res. Lett.* **22,** 3095–3098.

Murray, J., and P. Segall (2005). Spatiotemporal evolution of a transient slip event on the San Andreas fault near Parkfield, *J. Geophys. Res.* **110,** no. B09407, 1–12, doi 10.1029/2005JB003651.

Nadeau, R. M., and L. R. Johnson (1998). Seismological studies at Parkfield VI: Moment release rates and estimates of source parameters for small repeating earthquake, *Bull. Seismol. Soc. Am.* **88,** 790–814.

Nadeau, R. M., and T. V. McEvilly (1999). Fault slip rates at depth from recurrence intervals of repeating microearthquakes, *Science* **285,** 718–721.

Nadeau, R. M., W. Foxall, and T. V. McEvilly (1995). Clustering and periodic recurrence of microearthquakes on the San Andreas fault at Parkfield, California, *Science* **267,** 503–507.

Nadeau, R. M., A. Michelini, R. A. Uhrhammer, D. Dolenc, and T. V. McEvilly (2004). Detailed kinematics, structure and recurrence of micro-seismicity in the SAFOD target region, *Geophys. Res. Lett.* **31,** L12S08, doi 10.1029/2003GL019409.

Peng, Z., J. E. Vidale, C. Marone, and A. Rubin (2005). Systematic variations in recurrence interval and moment of repeating aftershocks, *Geophys. Res. Lett.* **32,** L15301, doi 10.1029/2005GL022626.

Rybicki, K., T. Kato, and K. Kasahara (1985). Mechanical interaction between neighboring active faults: Static and dynamic stress field induced by faulting, *Bull. Earthq. Res. Inst. Univ. Tokyo* **60,** 1–21.

Schaff, D. P., G. C. Beroza, and B. E. Shaw (1998). Postseismic response of repeating aftershocks, *Geophys. Res. Lett.* **25,** 4549–4552, doi 10.1029/1998GL900192.

Scholz, C. H. (1990). *The Mechanics of Earthquakes and Faulting*, Cambridge Univ. Press, New York, 439 pp.,

Stein, R. S. (1999). The role of stress transfer in earthquake occurrence, *Nature* **402,** 605–609.

Sykes, L. R., and W. Menke (2006). Repeat times of large earthquakes: Implications for earthquake mechanics and long-term prediction, *Bull. Seismol. Soc. Am.* **96,** 1569–1596, doi 10.1785/0120050083.

Trotta, J. E., and T. E. Tullis (2006). An independent assessment of the load/unload response ratio (LURR) proposed method of earthquake prediction, *Pure Appl. Geophys.* **163,** 2375–2387, doi 10.1007/s00024-006-0128-9.

Vidale, J. E., W. L. Ellsworth, A. Cole, and C. Marone (1994). Variations in rupture process with recurrence interval in a repeated small earthquake, *Nature* **368,** 624–626.

Wessel, P., and W. H. F. Smith (1998). New, improved version of the Generic Mapping Tools released, *EOS Trans. AGU*, **79,** 329.

Department of Earth Sciences
National Taiwan Normal University
No. 88, Sec. 4, Tingzhou Rd.
Wenshan District, Taipei, 116, Taiwan
(K.H.C.)

Berkeley Seismological Laboratory
University of California
Berkeley, California 94720-4760, USA
(R.B., R.M.N.)

Manuscript received 17 December 2008